Geochemical Perspectives Letters

Forty-year pollution history of microplastics in the largest marginal sea of the western Pacific

M. Chen, M. Du, A. Jin, S. Chen, S. Dasgupta, J. Li, H. Xu, K. Ta, X. Peng

Supplementary Information

The Supplementary Information includes:

- Study Area
- Sampling and Analytical Methods
- Tables S-1 to S-3
- Figures S-1 and S-2
- Supplementary Information References

Study Area

The study area is located in the northern South China Sea (SCS), which includes the northern continental shelf of SCS, the Xisha Canyon and the Xisha Trough. The depth of the continental shelf of SCS is shallower than 500 m, while the Xisha Trough lies near 18°N, trends EW and deepens eastwards from 1500 to 3400 m (Qiu *et al*., 2001), with horst-and-graben structures developed in the basement (Shi *et al*., 2002). The surface circulation of the SCS is mainly driven by the monsoon and has significant seasonal variations (Liu *et al*., 2008). There is a large cyclonic gyre in winter and a weak anticyclonic gyre remains in summer in the northern SCS (Liu *et al*., 2008). Figure 3a in the main text was produced in GMT version 5.4 (Wessel *et al*., 2013). Bathymetric data were downloaded from the NOAA national centers for environmental information (https://maps.ngdc.noaa.gov/viewers/wcs-client/.

Sampling and Analytical Methods

Sediment samples from the Xisha Canyon and the Xisha Trough were recovered using the pushcore sampler by manipulators during the TS-07 Cruise carried out via R/V TANSUOYIHAO with manned submersible *Shenhaiyongshi* from May to June 2018. Sediment samples from the continental shelf of SCS were collected using the box sampler during the cruise of R/V *Zhanke 10* in November, 2018. Pushcores that were used to collect sediments were made of transparent PVC. We did not detect transparent PVC in sediment samples in this study, showing these pushcores had no contaminations for sampling. After recovery, sediment samples were subsampled at 2 cm intervals and stored at -20 ˚C until further analysis. In the laboratory, frozen sediments from all the cores were defrosted, pooled and homogenised. Three subsamples were weighed before and after freeze-drying. The sediment extraction, purification, and identification were performed according to Peng *et al*. (2018). In brief, the saturated sodium chloride solution was added to separate microplastics from dried sediment. Then the samples were centrifuged and the supernatant was transferred and filtered over the Whatman glass fibre filter (GF/F, 47 mm). After filtration, the filter units were rinsed three times using deionised water. The remaining solids were resuspended in concentrated sodium iodide solution and the extraction procedure described

above was repeated. The filters were examined with an optical microscope (Leica stereoscope, LED5000 SLI) for the quantification of microplastics at the Institution of Deep-sea Science and Engineering, CAS. A LamRAM HR800 (JY/Horiba) Raman spectrometer were used to identify the type of microplastics at the Institution of Deep-sea Science and Engineering, CAS. In order to avoid high energy damage to samples, the energy of the spectrum was set up to below 10 %. The wavelength of the excitation laser and the spectral resolution of the Raman spectrometer was 532 nm and ~1.0 cm^{-1}, respectively. A Raman range of 200-3600 cm^{-1} was chosen for measurements. All spectra were acquired for 5-20 s with two to three accumulations per spectrum.

The activities of ^{137}Cs, ^{210}Pb, and ^{226}Ra in sediment samples were measured at the State Key Laboratory of Estuarine and Coastal Research at East China Normal University. The samples were freeze-dried and homogeneously pulverised, weighed, and then sealed in a plastic box (70 mm diameter x 70 mm height) for 3 weeks for radionuclide analysis. The activities of ^{210}Pbex and ^{137}Cs in sediment samples were measured following the method described by Du *et al*. (2008, 2010) and Wang *et al*. (2016). Radioactivity of the above nuclides was measured using an HPGe c ray detector with a relative counting efficiency of 35 % and an energy resolution of 1.8 keV (at 1332 keV) in multi-layer shielding of 15 cm Pb, 1 mm Cd, 1 mm Cu and 5 mm Plexiglas. The measuring times were between 4 and 24 h. The detector has multilayer shielding (ultralow cryostat and no peak background in the isotopes of interest). The activities of ^{137}Cs were determined from the c ray peak at 661.6 keV (85 %). The activity of ^{210}Pbex was calculated from the activity of a total ^{210}Pb (46.5 keV, 4.25 %) minus the activity of ^{226}Ra, determined using the c lines at 351.9 keV (37.6 %) for ^{214}Pb and 609.3 keV (46.1 %) for ^{214}Bi. To measure the activity of ^{226}Ra, the samples were sealed for at least 3 weeks to establish a secular equilibrium between ^{226}Ra and the daughter products of ^{222}Rn. The efficiency calibration of the detector systems was conducted using both the Laboratory Sourceless Calibration Software (LabSOCS) with efficiency uncertainties of 5–10 % (Baronson, 2003) and standard samples (GBW04127) to ensure the reliability of the QA/QC method. The deposition rates were calculated by CFCS model.

To avoid potential contamination, all alternative apparatus used were made of glass or stainless steel and thoroughly rinsed with Milli-Q water prior to use, all the polymer items possibly used in the processing were the same as Peng *et al*., (2018, Table S-3). All chemical solutions were filtered through polycarbonate filters (0.22 μm pore size, polyethersulfone, Merck Millipore) to remove particulate contaminants before use (Bergmann *et al*., 2017). Sample preparation was conducted within a super clean bench. To demonstrate the efficacy of our preventive measures, six procedural blanks and every air blank control group were run when counting to check for contamination (Hendrickson *et al*., 2018).

Supplementary Tables

Table S-1 Detailed information of sample stations.

Sample	Depth (m)	Longitude (°E)	Latitude (°N)	Type
SQW61	-1151	114.35	19.27	Pushcore
SQW38	-1182	112.01	17.75	Pushcore
SY81	-1366	110.40	16.69	Pushcore
SY79	-1377	110.41	16.73	Pushcore
SQW54	-1394	110.47	16.73	Pushcore
SQW44	-1445	110.53	17.30	Pushcore
SQW40	-1503	111.00	17.99	Pushcore
SY82	-1732	111.99	18.44	Pushcore
SQW43	-1741	111.03	17.60	Pushcore
SQW39	-1897	111.29	17.90	Pushcore
SY87	-2200	111.94	18.20	Pushcore
SY83	-2807	112.96	18.18	Pushcore
SY86	-3103	113.42	18.24	Pushcore
SY85	-3233	113.74	18.26	Pushcore
SY84	-3408	114.08	18.05	Pushcore
SQW31	-1581	110.97	17.10	Pushcore
SQW32	-1549	111.25	17.45	Pushcore
S00	-30	111.04	20.22	box
S01	-87	111.28	19.59	box
S02	-87	112.21	20.26	box
S03	-44	111.94	20.95	box
S04	-24	112.67	21.47	box
S05	-73	112.93	20.78	box
S11	-75	109.71	18.07	box

Table S-2 Dating results for sediment cores using ^{210}Pb dating method (ages in brackets were calculated valued according to the deposition rates).

Station	Deposition rate cm/yr	Years at the depth of cores									Source
		2 cm	4 cm	6 cm	8 cm	10 cm	12 cm	14 cm	16 cm	18 cm	
S00	0.47	2014	2009	2005	2001	1997	1992	1988	1984	1980	Li, 1988
S01	0.47	2014	2009	2005	2001	1997	1992	1988	1984	1980	Li, 1988
S02	0.36	2012	2005 (2007)	2001	1996	1992 (1990)	1985	1980 (1979)	1974	1968	Li, 1988
S03	0.50	2014	2010	2005 (2006)	2002	1998	1992 (1994)	1990	1986	1980 (1982)	This study
S04	0.49	2014	2010	2005 (2006)	2002	1998	1992 (1993)	1989	1985	1980 (1981)	This study
S05	0.36	2012	2005 (2007)	2001	1996	1992 (1990)	1985	1980 (1979)	1974	1968	Li, 1988
S11	0.47	2014	2009	2005	2001	1997	1992	1988	1984	1980	Li, 1988
SY83	0.15	2005	1992 (1991)	1980 (1977)	1963						This study
SY81	0.09	1992 (1995)	1980 (1971)	1948	1925						This study
SQW43	0.15	2005	1992	1980 (1979)	1966						This study
SY87	0.15	2005	1992 (1991)	1980 (1978)	1965						This study

Table S-3 ^{210}Pb dating results of S03, S04, SY83, SY81, SQW43 and SY87, stations.

Sample	Depth (cm)	Pb-210ex	error	Ra-226	error	Cs-137	error
S03	0-2	112.06	9.61	26.41	2.28	<LLD	
S03	3-4	102.63	5.52	27.04	1.34	<LLD	
S03	5-6	111.58	7.06	27.24	1.69	<LLD	
S03	7-8	105.81	5.70	24.90	1.34	0.72	0.39
S03	9-10	101.65	7.02	24.94	1.71	<LLD	
S03	11-12	73.41	5.23	26.05	1.31	1.06	0.36
S03	13-14	63.23	5.00	25.22	1.29	1.38	0.36
S03	15-16	56.73	5.51	29.82	1.46	<LLD	
S04	0-2	46.42	4.37	37.05	1.27	1.44	0.24
S04	3-4	54.55	3.93	34.58	1.11	0.96	0.28
S04	5-6	61.82	3.76	31.27	1.03	1.28	0.28
S04	7-8	63.87	5.17	34.98	1.43	2	0.38
S04	9-10	69.14	4.52	35.48	1.24	2.08	0.33
S04	11-12	72.01	4.21	35.8	1.17	0.71	0.31
S04	13-14	58.62	4.68	35.9	1.32	2.65	0.35
S04	15-16	40.23	4.16	34.93	1.18	1.69	0.31
S04	17-18	62.29	4.43	32.45	1.26	1.64	0.27
S04	19-20	48.72	4.41	37.11	1.26	2.18	0.35
S04	21-22	50.6	5.34	37.85	1.53	1.62	0.43
S04	23-24	39.76	4.52	35.57	1.29	1.33	0.35
SY83	0-2	191.98	12.71	75.58	3.56	<LLD	
SY83	3-4	67.28	10.98	72.22	3.63	<LLD	
SY83	5-6	98.91	11.75	82.09	3.75	<LLD	
SY83	7-8	72.59	5.82	85.51	1.91	<LLD	
SY83	9-10	76.74	9.70	116.37	3.33	<LLD	
SY83	13-14	38.25	8.58	74.82	3.06	<LLD	
SY83	17-18	6.22	8.16	74.81	2.92	<LLD	
SY81	0-2	318.99	10.60	45.38	2.73	<LLD	
SY81	3-4	202.21	11.48	48.86	3.04	<LLD	
SY81	5-6	75.90	9.66	45.11	3.22	<LLD	
SY81	9-10	9.76	5.18	34.91	1.64	<LLD	
SY81	11-12	9.25	5.46	32.83	1.73	<LLD	
SY81	13-14	8.23	6.08	34.63	1.88	<LLD	
SQW43	3-4	106.06	9.77	84.87	3.49	<LLD	
SQW43	5-6	191.92	8.91	98.39	3.00	<LLD	
SQW43	7-8	62.58	11.99	115.38	4.69	<LLD	
SQW43	9-10	54.40	9.22	68.40	3.31	<LLD	
SQW43	11-12	65.08	9.71	81.48	3.50	<LLD	
SQW43	13-14	30.97	11.80	91.99	4.49	<LLD	
SQW43	17-18	34.25	13.76	119.41	5.21	<LLD	
SY87	0-2	262.15	19.51	127.89	6.46	<LLD	
SY87	3-4	63.47	13.24	94.50	4.81	<LLD	
SY87	5-6	92.97	11.14	123.03	4.09	<LLD	
SY87	7-8	75.52	15.00	109.51	5.55	<LLD	
SY87	13-14	71.97	7.64	74.08	2.60	<LLD	
SY87	17-18	9.90	7.95	70.76	2.87	<LLD	
SY87	23-24	21.23	10.47	70.80	3.70	<LLD	

Supplementary Figures

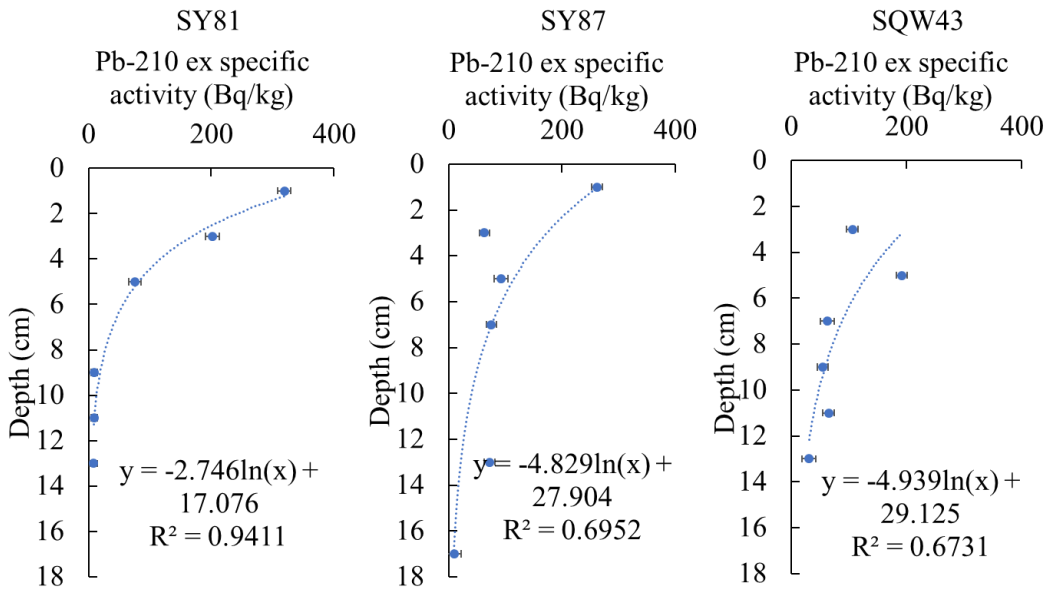

Figure S-1 The profiles of excess ^{210}Pb of sediment cores at SY81, SY87, and SQW43 stations. The sediment rates were calculated according to the gradient of the excess ^{210}Pb and the depth.

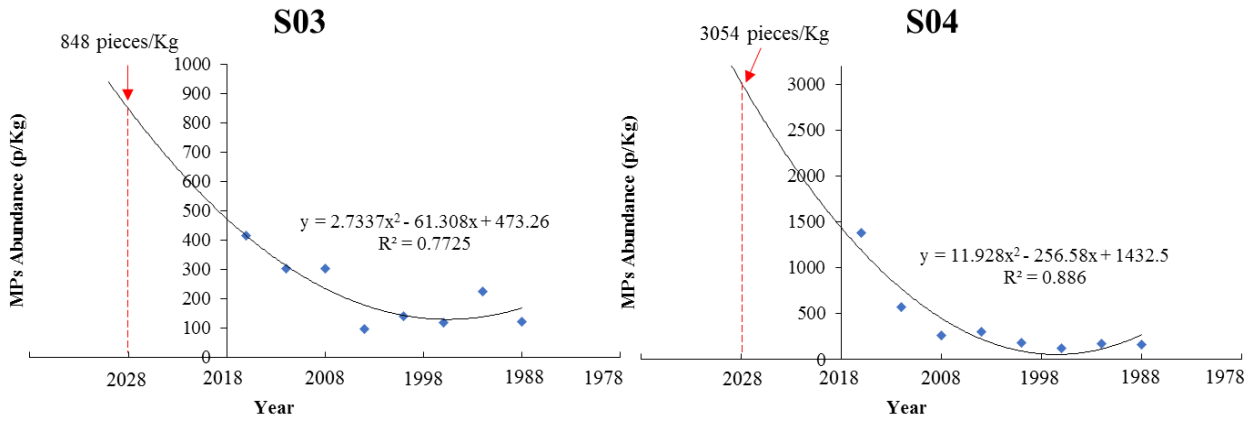

Figure S-2 Estimation based on the polynomial regression method shows that the microplastic abundance of microplastics in the surface sediments of S03 station and S04 station in 2028 (red arrows) will increase nearly two times as much as those in 2018.

Supplementary Information References

Baronson, F.L. (2003) Validation of the accuracy of the LabSOCS software for mathematical efficiency calibration of Ge detectors for typical laboratory samples. *Journal of Radioanalytical Nuclear Chemistry* 255, 137-141.

Bergmann, M., Wirzberger, V., Krumpen, T., Lorenz, C., Primpke, S., Tekman, M. B., Gerdts, G. (2017) High Quantities of Microplastic in Arctic Deep-Sea Sediments from the HAUSGARTEN Observatory. *Environmental Science & Technology* 51, 11000-11010.

Du, J., Wu, Y., Huang, D., Zhang, J. (2010) Use of ^{7}Be, ^{210}Pb and ^{137}Cs tracers to the transport of surface sediments of the Changjiang Estuary, China. *Journal of Marine Systems* 82, 286-294.

Du, J., Zhang, J., Wu, Y. (2008) Deposition patterns of atmospheric ^{7}Be and ^{210}Pb in coast of East China Sea, Shanghai, China. *Atmospheric Environment* 42, 5101-5109.

Hendrickson, E., Minor, E. C., Schreiner, K. (2018) Microplastic abundance and composition in western Lake Superior as determined via microscopy, Pyr-GC/MS, and FTIR. *Environmental Science & Technology* 52, 1787-1796.

Li, F. (1988) Determination of recent sedimentation rates by 210Pb method in the South China Sea. *Marine Sciences* 3, 64-66. (In Chinese with English Abstract).

Liu, Q.Y., Kaneko, A., Jilan, S. (2008) Physical recent progress in studies of the South China Sea circulation. *Journal of Oceanography* 64, 753-762.

Peng, X., Chen, M., Chen, S., Dasgupta, S., Xu, H., Ta, K., Li, J., Li, Guo, Z., Bai, S. (2018) Microplastics contaminate the deepest part of the world's ocean. *Geochemical Perspectives Letters* 9, 1-5.

Qiu, X., Ye, S., Wu, S., Shi, X., Zhou, D., Xia, K. (2001) Crustal structure across the Misha trough, northwestern south china sea. *Tectonophysics* 341, 179-193.

Shi, X., Zhou, D., Qiu, X., Zhang, Y. (2002) Thermal and rheological structures of the xisha trough, south china sea. *Tectonophysics* 351, 285-300.

Wang, J., Du, J., Baskaran, M., Zhang, J. (2016) Mobile mud dynamics in the east china sea elucidated using ^{210}Pb, ^{137}Cs, ^{7}Be, and ^{234}Th as tracers. Journal of Geophysical Research: Oceans 121, 224-239.

Wessel, P., Smith, W. H., Scharroo, R., Luis, J., Wobbe, F. (2013) Generic mapping tools: improved version released. *Eos, Transactions American Geophysical Union* 94, 409-410.